Performance evaluation of a simple feed-forward deep neural network model applied to annual rainfall anomaly index (RAI) over Indramayu, Indonesia

Sandy H. S. Herho[1, 2, *], Dasapta E. Irawan[3], Faiz R. Fajary[4, 5], Rusmawan Suwarman[5], and Siti N. Kaban[6]

[1]Department of Earth and Planetary Sciences, University of California, Riverside
[2]Department of Geology, University of Maryland, College Park
[3]Applied Geology Research Group, Bandung Institute of Technology
[4]Coastal Hazards and Energy System Science Lab, Hiroshima University
[5]Atmospheric Science Research Group, Bandung Institute of Technology
[6]School of Architecture, Planning, and Preservation, University of Maryland, College Park
[*]Corresponding author: sandy.herho@email.ucr.edu

June 30, 2023

Abstract

Indramayu is a district in West Java that is known for being the leading producer of rice and brackish salt. The production of these two commodities is strongly influenced by hydroclimatological conditions, making accurate and reliable long-term estimates crucial. In this study, we evaluated a simple feed-forward deep neural network (DNN) model that could potentially be used as a candidate for statistical guidance to improve the accuracy of numerical climate models.

We used the spatial average of the accumulated annual rainfall of the Climate Hazards Group InfraRed Precipitation with Station (CHIRPS) data as an input time series with a time range from 1981 to 2022. This data was then processed into annual rainfall anomaly index (RAI) data. The Annual RAI was divided into training and test sets, and the feed-forward DNN model was fitted to the annual RAI in the training set. The accuracy of the model was then tested in the test set using the root-mean-square error (RMSE) metric.

Our study shows that the feed-forward DNN model is not suitable for estimating the annual RAI over Indramayu. This is because the RMSE values are significantly high in both the training and test sets.

1 Introduction

Indramayu is a district located in the northern coastal area (Pantura) of West Java, approximately 190 km east of Jakarta. Topographically, Indramayu is a lowland area with an elevation ranging from 5 to 20 meters above sea level (m.a.s.l.) and a slope between 0 to 2% (1; 2) (Figure 1).

Geologically, Indramayu is classified as part of the alluvial plain of northern Java in the tectono-physiographic zoning division of West Java (3; 4). Its surface geology consists of river deposits, coastal deposits, deltaic deposits, flood-plain deposits, tufaceous sandstone and conglomerate, and beach-ridge deposits, all of which are of Quaternary age (2).

According to the study of rainfall delineation over the Maritime Continent conducted by Aldrian and Susanto (5), Indramayu is classified as Region A. This region has an average annual precipitation with one peak between November to March and one trough between May to September due to the movement of the northwest and southeast monsoons (Figure 2).

Indramayu is known for being one of the largest areas in West Java for producing rice and brackish salt (6; 7; 8). However, the sustainability of these commodities is threatened by hydroclimatological disasters such as floods and droughts (9). It is therefore necessary to adapt to and mitigate these disasters. Additionally, greenhouse gas levels are increasing at an unprecedented rate, which is projected to increase hydroclimatological disasters (10).

To prepare for this, local hydroclimatological projections need to be evaluated quantitatively so that local government agencies can make use of them. One way to make these projections is by using a mesoscale climate numerical model for an area the size of the Indramayu District (11; 12). However, this can be difficult due to the distinct cloud mixture properties that occur in tropical regions (13).

In this study, we evaluated the feasibility of using the annual rainfall anomaly index (RAI) statistical model, based on feed-forward deep neural networks (DNN), as a candidate for providing statistical guidance (14) on mesoscale numerical models. This can help produce more realistic long-term hydroclimatological projections in Indramayu.

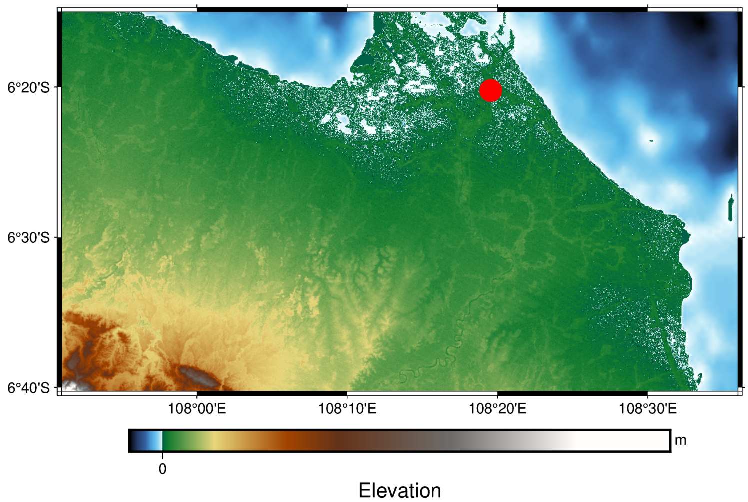

Figure 1: Study area representing the digital elevation model (DEM) of Indramayu District (rendered using **PyGMT** library (15; 16)). The red dot indicates the capital city, located at $108°\ 19'\ 27.6276''$E, $6°\ 21'\ 10.0728''$S.

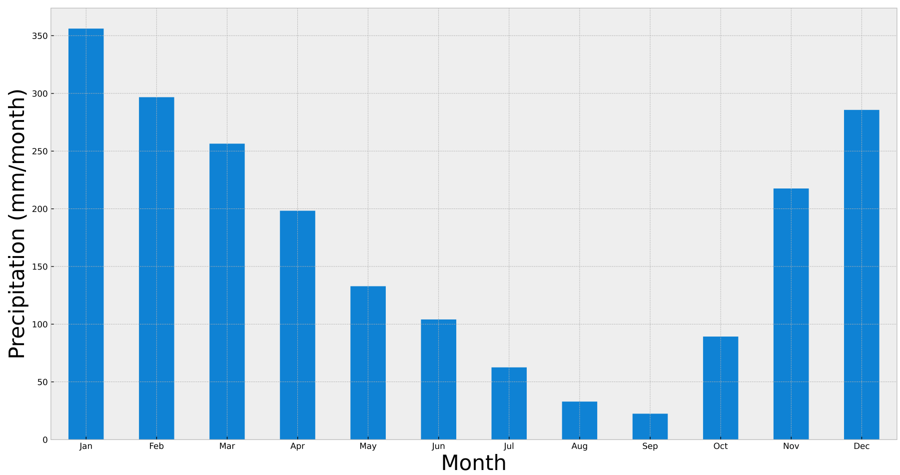

Figure 2: 1981 - 2022 average annual precipitation by month in Indramayu from CHIRPS dataset (17; 18).

2 Data and Methods

2.1 Data

In this study, we used quasi-global monthly precipitation from the Climate Hazards Group InfraRed Precipitation with Station data (CHIRPS) dataset (17; 18) with a spatial resolution of $0.05° \times 0.05°$ (`https:`

//data.chc.ucsb.edu/products/CHIRPS-2.0/ accessed on 19 June 2023) from 1981 to 2022. This dataset was sliced to the Indramayu District grids ($108°$' - $108°36'$E, $6°40'$ - $6°15'$S). Based on previous studies (e. g. 19; 20; 21; 22), we used this dataset because the CHIRPS dataset shows a reasonably good performance in representing precipitation over the Maritime Continent.

2.2 Methods

2.2.1 RAI calculation

We used RAI (23) as an index to describe rainfall anomalies over Indramayu. RAI is a simple meteorological drought/wetness index widely used as an alternative to more complex hydroclimatological indexes such as the standardized precipitation index (SPI) and standardized precipitation-evapotranspiration index (SPEI) (24; 25).

In addition, RAI has also been demonstrated to be capable of characterizing hydrometeorological drought in one of the areas over the Maritime Continent, namely in Kupang, East Nusa Tenggara (26).

The following is the equation that we used to calculate the annual RAI over Indramayu, where R is the current annual precipitation amount, $\overline{R}$ is the average annual precipitation from 1981 to 2022, M is the average of the 90th percentile, and N is the average of the 10th percentile. Before calculating the annual RAI, we first accumulated the monthly precipitation dataset into an annual format using the **xarray** library (27).

$$\text{RAI} = \begin{cases} 3\left(\frac{R-\overline{R}}{M-\overline{R}}\right) & \text{, for } R > \overline{R} \\ -3\left(\frac{R-\overline{R}}{X-\overline{R}}\right) & \text{, for } R < \overline{R}. \end{cases} \tag{1}$$

2.2.2 Data Preprocessing

To preprocess the spatiotemporal RAI dataset, we first took the spatial average of the dataset. Next, using the **xarray** library, we transformed the dataset, which was still a `DataArray` object, into a `DataFrame` object in **pandas** library (28). We then added a third-degree polynomial feature to the time index to capture nonlinearity in the dataset (29; 30). This was done automatically using the `PolynomialFeatures()` function in the **scikit-learn** library (31). Finally, we separated the data into 80% for training (1981-2013) and 20% for testing (2014-2022).

2.2.3 Model Development and Fitting

The statistical model used in this study is the DNN model. Based on the universal approximation theorem (29), this model can approximate any continuous function if given the right combination of inputs, weights, and biases. Furthermore, due to the development of the graphics processing unit (GPU) and the success of AlexNet (30), DNN is now widely used to solve problems in all fields of science. In hydrology, for example, it is currently a trend to predict dryness/wetness indexes statistically using DNN (e. g. 31; 32; 33; 34; 35; 36).

We chose a feed-forward DNN architecture for our model, consisting of one input layer, three hidden layers, and one output layer. The input layer has three neurons, which resulted from scaling the third-degree polynomial feature. Each hidden layer contains 100 neurons, and the output layer has only one neuron. We used dense and fully connected layers. This architecture was selected for its success in projecting statistical long-term CO_2 increases (37) (Figure 3). The feed-forward DNN was chosen to align with Occam's Razor, which states that the simplest model with the best predictability power should be selected (38; 39). After transforming the features in the dataset into the third-degree polynomial, we entered them as input xi into the DNN feed-forward architecture (Figure 3). They were then multiplied by the weight w_i and added with bias b, resulting in the output prediction $\hat{y}$. This process is illustrated in the following set of equations.

$$\begin{cases} z = \sum_{i=1}^{N} x_i w_i + b \\ \hat{y} = \sigma(z) \end{cases} \tag{2}$$

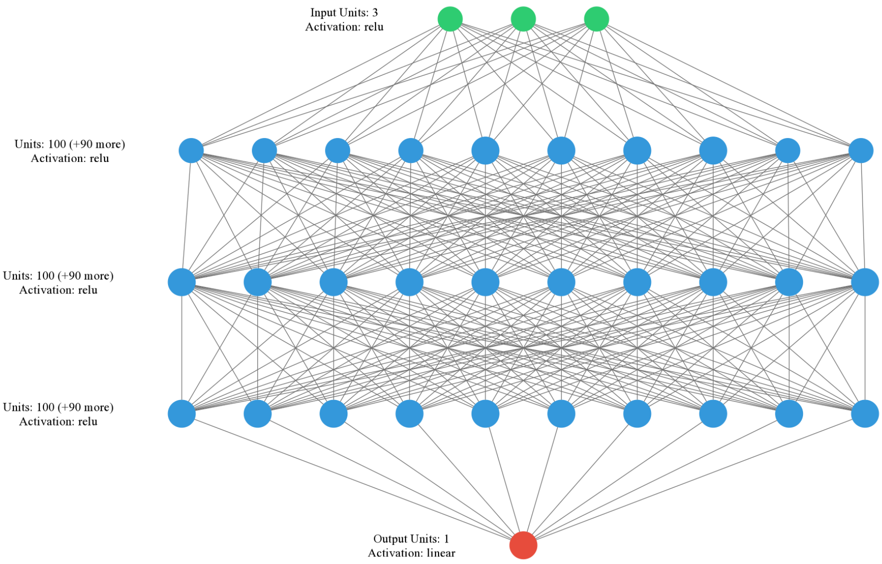

Figure 3: Architecture of a simple feed-forward DNN used in this study (rendered using **keras-visualizer** library (40)).

This study utilized rectified linear units (ReLU) as the activation function σ for each layer. ReLU offers several advantages over the sigmoid activation function: it avoids the vanishing gradient problem, is computationally more efficient (as it only specifies a maximum value between 0 and z), and exhibits better convergence performance than sigmoid (41; 42).

After obtaining the temporary output, we used the backpropagation procedure to optimize the weights and biases. This is done using the cost function $\mathcal{C}$, which is based on the weights and biases in each layer and is calculated using the following equation,

$$\mathcal{C} = -\ln(\hat{y}) \tag{3}$$

The gradient was calculated by working backward through the cost function, considering the weights and biases in each layer until the input layer was reached. This gradient, along with the cost function, was used to optimize the parameters in the feed-forward DNN architecture using a gradient-descent-based optimization algorithm (43). Set of equations 4 and 5 illustrate this process.

$$\begin{cases} \frac{\partial \mathcal{C}}{\partial \hat{y}} = -\frac{1}{\hat{y}} \\ \frac{\partial \hat{y}}{\partial z} = \sigma'(z) \\ \frac{\partial z}{\partial w_i} = x_i \\ \frac{\partial z}{\partial b} = 1 \end{cases} \tag{4}$$

$$\begin{cases} \frac{\partial \mathcal{C}}{\partial b} = \frac{\partial \mathcal{C}}{\partial \hat{y}} \frac{\partial \hat{y}}{\partial z} \frac{\partial z}{\partial b} \\ \frac{\partial \mathcal{C}}{\partial w_i} = \frac{\partial \mathcal{C}}{\partial \hat{y}} \frac{\partial \hat{y}}{\partial z} \frac{\partial z}{\partial w_i} \end{cases} \tag{5}$$

When updating the network weights, it is necessary to decrease the gradient. This decrease aims to minimize the network's cost function by shifting the hyperparameters along the negative gradient direction.

The gradient is a vector that stores all partial derivatives of the hyperparameter functions. At each iteration step (epoch), the model's hyperparameters are updated according to the following rules.

$$\begin{cases} w^* := w_i - \alpha \frac{\partial \mathcal{C}}{\partial w_i} \\ b^* := b_i - \alpha \frac{\partial \mathcal{C}}{\partial b_i} \end{cases} \tag{6}$$

Here, w_i and b_i are the updated weights and biases, w and b are the current weights and biases, $\mathcal{C}$ is the cost function, and α is the learning rate (0.001). In this study, the Adam optimizer algorithm was used for this process. The entire process of building and fitting this model to the training and test data was done automatically using the **Keras** interface (44) in the **TensorFlow** library (45).

2.2.4 Model Evaluation

We used the root-mean-square error (RMSE) (equation 7) to evaluate the accuracy of the RAI estimates from the feed-forward DNN on both the training and test data.

$$\text{RMSE} = \sqrt{\frac{\sum_{i=1}^{N}(y_i - \hat{y}_i)^2}{N}} \tag{7}$$

Here, N represents the total number of years in the time series, y_i represents the actual RAI observations, and $\hat{y}_i$ represents the estimated RAI from our feed-forward DNN algorithm. To evaluate the overfitting of the model, we used equation 8.

$$\varepsilon = \frac{(\text{RMSE}_{\text{test}} - \text{RMSE}_{\text{train}})}{\text{RMSE}_{\text{train}}} \times 100\% \tag{8}$$

ε is the ratio of the RMSE on test data to the RMSE on training data. If ε is very large, then it may indicate that the model is overfitted. The next step is to compare our model with a naïve model as a benchmark (46; 47). In this case, we compared the test RMSE of the DNN feed-forward model with that of a simple model that assumes the estimated RAI value in the following year is the same as the actual RAI value in the previous year. The equation for this model is shown below.

$$\hat{y}_{i+1} = y_i \tag{9}$$

Following the Occam's Razor principle discussed earlier, if the test RMSE on the naïve model is better than the test RMSE of the model we built, then we can conclude that the feed-forward DNN fails to predict the annual RAI over Indramayu. The final step is to assess the model's sensitivity to hyperparameters. This involves varying the number of epochs and neurons in the hidden layers and changing the degree of polynomial features (37). Finally, we compare the test RMSEs of these models with the initial feed-forward DNN architecture.

3 Results and Discussion

Figure 4 shows the evolution of the spatial average of RAI over Indramayu. In 1997, there was a severe drought event with a spatial average of RAI -3.65, which falls under the extremely dry category (23) (Figure 5a). This event coincided with one of the most significant El Niño Southern Oscillation (ENSO) and Indian Ocean Dipole (IOD) positive anomalies of the 20th century, resulting in many droughts, forest fires, and the death of coral reefs in the Maritime Continent (48; 49; 50; 51).

On the other hand, the wettest event occurred in 2016 (Figure 5), when the spatial average of RAI over Indramayu reached 4.05, classified as extremely wet (23). This event coincided with a strong negative IOD and weak La Niña events (52; 53; 54). .

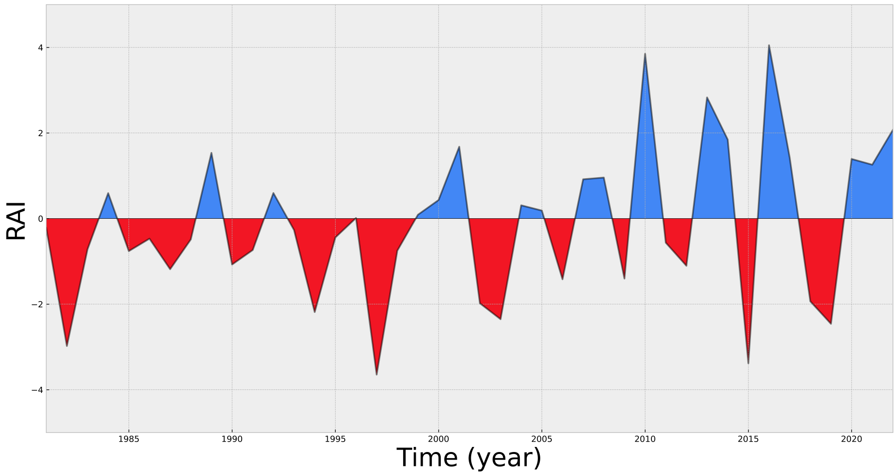

Figure 4: Evolution of the annual RAI over Indramayu from 1981 to 2022.

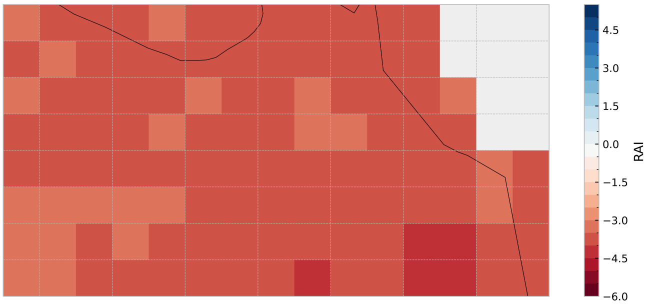

(a)

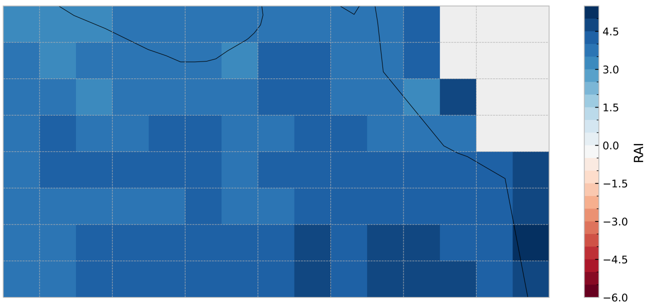

(b)

Figure 5: Spatial maps of the annual RAI over Indramayu during (a) the driest event (1997) and (b) the wettest event (2016). The gray area is the Java Sea, where precipitation data was intentionally not included in the dataset.

The graph in Figure 6 shows the values of the mean squared error (MSE) loss function relative to the number of iterations (100 epochs) when fitting the DNN feed-forward architecture (Figure 3) to the RAI training data from 1981 to 2013. The MSE slopes in the range of $0.7 - 0.8$ after the 60th epoch. The input and three hidden layers of the model contain a total of 20,701 hyperparameters that were trained.

However, the estimation results of the model on training data have a root mean squared error (RMSE) of 132.9%, and the RMSE on test data is 259.58% with the comparison testing - training parameter of 96.07%. The large RMSE on both the training and test data suggests that the feed-forward DNN architecture we developed failed to accurately estimate the annual RAI in Indramayu. Furthermore, the significant difference between the RMSE on the test data and the training RMSE indicates the possibility of overfitting.

This fact is also supported by the feed-forward DNN's ability to estimate drought events due to El Niño in 1997, which was within the training set range, while failing to estimate extreme drought and wetness in 2015-2016, which were outside the training set (Figure 7). However, our sensitivity test results showed no significant change in the test RMSE, even though we varied the number of hyperparameters in each hidden layer (Table 1). Therefore, the feed-forward DNN architecture we used failed to provide a realistic estimate of the annual RAI in Indramayu using annual input data for the 42 years from 1981 to 2022.

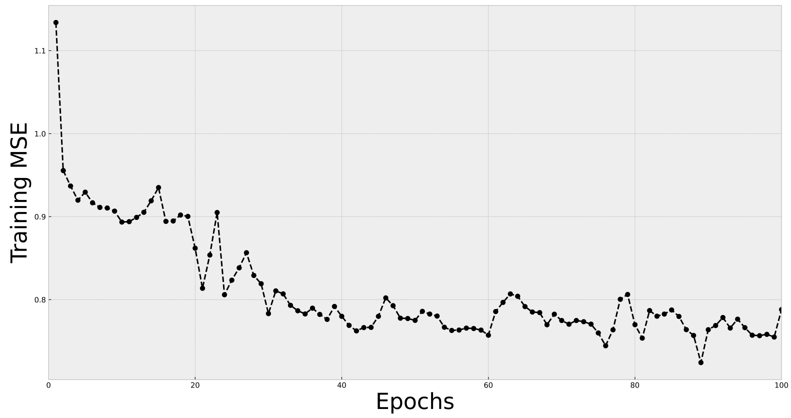

Figure 6: Training MSE for 100 epochs.

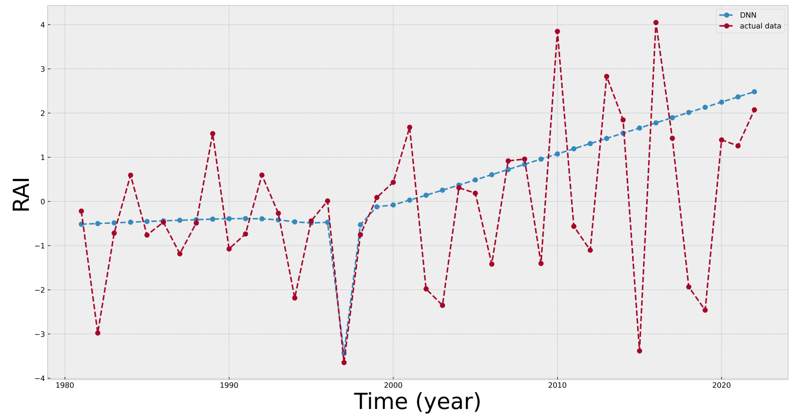

Figure 7: Comparison of two time series between actual RAI observations (red line) and RAI estimated results from fitting the feed-forward DNN model on the training data (blue line).

Table 1: Test RMSE using different hyperparameters in the original feed-forward DNN architecture.

polynomial degree	epochs	number of neurons per hidden layer	test RMSE
1	50	50	233.32 %
1	50	100	233.57 %
1	100	50	238.67 %
1	100	100	239.89 %
2	50	50	232.95 %
2	50	100	232.98 %
2	100	50	239.87 %
2	100	100	239.25 %

4 Conclusion and Outlooks

Based on the annual RAI data currently used in Indramayu, we conclude that our simple feed-forward DNN algorithm did not produce an accurate estimation. Hyperparameter tuning did not improve the accuracy of this model either. To test the accuracy of this algorithm in the future, more data points are needed. However, we can also try using another statistical model that is simpler and more transparent than our DNN model to get a more accurate estimate. One candidate that can be tested for future studies is the Bayesian structural time series (BSTS) model (55), as demonstrated by Herho et al. (56), which presented a reasonably accurate statistical estimate of the quite noisy monthly station precipitation data from the Natuna Islands. Moreover, BSTS provides prior belief features that can be easily assimilated with estimates from mesoscale climate models and exogenous features (covariates), which can be filled with large-scale climate indices considered to affect the annual RAI in Indramayu. In addition, we can also take advantage of a more comprehensive annual rainfall dataset in areas with the same climatic characteristics as Indramayu, for example, Jakarta, to train our feed-forward DNN model, which is then used to estimate the annual RAI over Indramayu. This transfer learning method is widely used for runtime constraints when training models and data imputation in time series studies in hydrology and environmental sciences (e.g. 57; 58; 59; 60; 61).

Open Research

The quasi-global monthly CHIRPS dataset can be downloaded at `https://data.chc.ucsb.edu/products/CHIRPS-2.0/`. Although the entire analysis can be made using publicly available data, the intermediate data required for the main analysis, as well as Python code are freely available at `https://github.com/sandyherho/IndraAnnDeepEval`.

Acknowledgments

Spyros Giannelos (Imperial College London) was acknowledged for providing valuable discussion. This study was supported by ITB Research, Community Service and Innovation Program (P3MI-ITB).

References

[1] A. F. Rusydi, S.-I. Onodera, M. Saito, S. Ioka, and R. Maria, "Estimation of ammonium sources in Indonesian coastal alluvial groundwater using Cl- and GIS," *International Journal of GEOMATE*, vol. 17, no. 62, pp. 53–58, 2019.

[2] A. F. Rusydi, S.-I. Onodera, M. Saito, S. Ioka, R. Maria, I. Ridwansyah, and R. M. Delinom, "Vulnerability of groundwater to iron and manganese contamination in the coastal alluvial plain of a developing Indonesian city," *SN Applied Sciences*, vol. 3, pp. 1–12, 2021.

[3] R. W. van Bemmelen, "General Geology of Indonesia and adjacent archipelagoes," *The geology of Indonesia*, 1949.

[4] R. M. Delinom, "Structural geology controls on groundwater flow: Lembang Fault case study, West Java, Indonesia," *Hydrogeology Journal*, vol. 17, no. 4, pp. 1011–1023, 2009.

[5] E. Aldrian and R. D. Susanto, "Identification of three dominant rainfall regions within Indonesia and their relationship to sea surface temperature," *International Journal of Climatology*, vol. 23, no. 12, pp. 1435–1452, 2003.

[6] S. H. S. Herho, G. A. Firdaus, and P. M. Siregar, "Pengaruh Aspek Meteorologi Terhadap Produksi Garam Air Payau di Desa Losarang, Kabupaten Indramayu [The Influence of Meteorological Aspects on Brackish Water Salt Production in Losarang Village, Indramayu Regency]," in *Prosiding Seminar Nasional dan Rapat Tahunan MIPAnet: Sains untuk Kehidupan [Proceedings of the MIPAnet National Seminar and Annual Meeting: Sciences for Life]* (F. R. Mantiri, D. Hatidja, N. Nainggolan, H. Aritonang, and C. Montolalu, eds.), pp. 341 – 352, September 2017.

[7] A. I. Setianingsih, M. Jalaludin, and W. Warnadi, "Analysis droughts index by Standardized Precipitation Index (SPI) and productivity of rain-fed rice fields in Indramayu West Java," *Journal of Physics: Conference Series*, vol. 1469, no. 1, p. 012111, 2020.

[8] H. Ajiwibowo and M. B. Pratama, "EVALUATION OF MUD SETTLING POND PERFORMANCE IN A SALT POND ENVIRONMENT IN LOSARANG DISTRICT, REGENCY OF INDRAMAYU, WEST JAVA, INDONESIA," *International Journal of GEOMATE*, vol. 23, p. 97–103, 2022.

[9] P. D'Odorico, F. Laio, and L. Ridolfi, "Does globalization of water reduce societal resilience to drought?," *Geophysical Research Letters*, vol. 37, no. 13, p. L13403, 2010.

[10] IPCC, *Climate Change 2021: The Physical Science Basis. Contribution of Working Group I to the Sixth Assessment Report of the Intergovernmental Panel on Climate Change*. Cambridge, UK and New York, NY, USA: Cambridge University Press, 2021.

[11] I. Orlanski, "A rational subdivision of scales for atmospheric processes," *Bulletin of the American Meteorological Society*, pp. 527–530, 1975.

[12] R. A. Houze Jr., "Mesoscale convective systems," *Reviews of Geophysics*, vol. 42, no. 4, p. RG4003, 2004.

[13] W. B. Rossow, G. Tselioudis, A. Polak, and C. Jakob, "Tropical climate described as a distribution of weather states indicated by distinct mesoscale cloud property mixtures," *Geophysical Research Letters*, vol. 32, no. 21, p. L21812, 2005.

[14] G. M. Carter, J. P. Dallavalle, and H. R. G., "Statistical forecasts based on the national meteorological center's numerical weather prediction system," *Weather and Forecasting*, vol. 4, no. 3, pp. 401 – 412, 1989.

[15] P. Wessel, J. F. Luis, L. Uieda, R. Scharroo, F. Wobbe, W. H. F. Smith, and D. Tian, "The Generic Mapping Tools Version 6," *Geochemistry, Geophysics, Geosystems*, vol. 20, no. 11, pp. 5556–5564, 2019.

[16] L. Uieda, D. Tian, W. J. Leong, W. Schlitzer, M. Grund, M. Jones, Y. Fröhlich, L. Toney, J. Yao, Y. Magen, J.-H. Tong, K. Materna, A. Belem, T. Newton, A. Anant, M. Ziebarth, J. Quinn, and P. Wessel, "PyGMT: A Python interface for the Generic Mapping Tools," 2023. Software available from `https://doi.org/10.5281/zenodo.7772533`.

[17] C. Funk, P. Peterson, M. Landsfeld, D. Pedreros, J. Verdin, S. Shukla, G. Husak, J. Rowland, L. Harrison, A. Hoell, *et al.*, "The climate hazards infrared precipitation with stations—a new environmental record for monitoring extremes," *Scientific data*, vol. 2, no. 1, pp. 1–21, 2015.

[18] C. Funk, P. Peterson, S. Peterson, S. Shukla, F. Davenport, J. Michaelsen, K. R. Knapp, M. Landsfeld, G. Husak, L. Harrison, *et al.*, "A high-resolution 1983–2016 t max climate data record based on infrared temperatures and stations by the climate hazard center," *Journal of Climate*, vol. 32, no. 17, pp. 5639–5658, 2019.

[19] D. Auliyani and N. Wahyuningrum, "Rainfall variability based on the Climate Hazards Group InfraRed Precipitation with Station Data (CHIRPS) in Lesti watershed, Java Island, Indonesia," *IOP Conference Series: Earth and Environmental Science*, vol. 874, no. 1, p. 012003, 2021.

[20] I. Narulita, F. R. Fajary, A. Mulyono, E. Kusratmoko, and M. R. Djuwansah, "Application of Climate Hazards Group InfraRed Precipitation with Station (CHIRPS) satellite data for drought mitigation in Bintan island, Indonesia," *IOP Conference Series: Earth and Environmental Science*, vol. 789, no. 1, p. 012052, 2021.

[21] I. Narulita, F. R. Fajary, M. R. Syahputra, E. Kusratmoko, and M. R. Djuwansah, "Spatio-temporal rainfall variability of equatorial small island: case study bintan island, indonesia," *Theoretical and Applied Climatology*, vol. 144, pp. 625–641, 2021.

[22] S. Wahyuni, D. Sisinggih, and I. A. G. Dewi, "Validation of Climate Hazard Group InfraRed Precipitation with Station (CHIRPS) Data in Wonorejo Reservoir, Indonesia," *IOP Conference Series: Earth and Environmental Science*, vol. 930, no. 1, p. 012042, 2021.

[23] M. P. Van Rooy, "A Rainfall Anomaly Index (RAI), Independent of the Time and Space," *Notos*, vol. 14, pp. 43 – 48, 1965.

[24] T. Raziei, "Revisiting the rainfall anomaly index to serve as a simplified standardized precipitation index," *Journal of Hydrology*, vol. 602, p. 126761, 2021.

[25] A. Aryal, M. Maharjan, R. Talchabhadel, and B. R. Thapa, "Characterizing Meteorological Droughts in Nepal: A Comparative Analysis of Standardized Precipitation Index and Rainfall Anomaly Index," *Earth*, vol. 3, no. 1, pp. 409–432, 2022.

[26] S. H. S. Herho and G. A. Firdaus, "Time-series analysis and statistical forecasting of daily rainfall in Kupang, East Nusa Tenggara, Indonesia," *International Journal of Data Science*, vol. 3, no. 1, pp. 25–32, 2022.

[27] S. Hoyer and J. Hamman, "xarray: ND labeled arrays and datasets in Python," *Journal of Open Research Software*, vol. 5, no. 1, 2017.

[28] W. McKinney, "Data Structures for Statistical Computing in Python," in *Proceedings of the 9th Python in Science Conference* (S. van der Walt and J. Millman, eds.), pp. 56 – 61, 2010.

[29] Y. Lu and J. Lu, "A Universal Approximation Theorem of Deep Neural Networks for Expressing Probability Distributions," in *Advances in Neural Information Processing Systems* (H. Larochelle, M. Ranzato, R. Hadsell, M. Balcan, and H. Lin, eds.), vol. 33, pp. 3094–3105, Curran Associates, Inc., 2020.

[30] A. Krizhevsky, I. Sutskever, and G. E. Hinton, "ImageNet Classification with Deep Convolutional Neural Networks," in *Advances in Neural Information Processing Systems* (F. Pereira, C. Burges, L. Bottou, and K. Weinberger, eds.), vol. 25, Curran Associates, Inc., 2012.

[31] S. Azimi and M. A. Moghaddam, "Modeling short term rainfall forecast using neural networks, and Gaussian process classification based on the SPI drought index," *Water Resources Management*, vol. 34, pp. 1369–1405, 2020.

[32] X. Liu, X. Zhu, Q. Zhang, T. Yang, Y. Pan, and P. Sun, "A remote sensing and artificial neural network-based integrated agricultural drought index: Index development and applications," *Catena*, vol. 186, p. 104394, 2020.

[33] A. Anshuka, A. J. V. Buzacott, R. W. Vervoort, and F. F. van Ogtrop, "Developing drought index–based forecasts for tropical climates using wavelet neural network: an application in Fiji," *Theoretical and Applied Climatology*, vol. 143, pp. 557–569, 2021.

[34] A. Dikshit, B. Pradhan, and A. Huete, "An improved SPEI drought forecasting approach using the long short-term memory neural network," *Journal of environmental management*, vol. 283, p. 111979, 2021.

[35] O. O. Evkaya and F. S. Kurna, "Forecasting drought using neural network approaches with transformed time series data," *Journal of Applied Statistics*, vol. 48, no. 13-15, pp. 2591–2606, 2021.

[36] A. Dikshit, B. Pradhan, and M. Santosh, "Artificial neural networks in drought prediction in the 21st century–A scientometric analysis," *Applied Soft Computing*, vol. 114, p. 108080, 2022.

[37] S. Giannelos, A. Moreira, D. Papadaskalopoulos, S. Borozan, D. Pudjianto, I. Konstantelos, M. Sun, and G. Strbac, "A Machine Learning Approach for Generating and Evaluating Forecasts on the Environmental Impact of the Buildings Sector," *Energies*, vol. 16, no. 6, 2023.

[38] S. H. S. Herho, *Pijar Filsafat Yunani Klasik [Glow of Classical Greek Philosophy]*. Bandung, Indonesia: PSIK ITB, 2016.

[39] S. V. Weijs and B. L. Ruddell, "Debates: Does Information Theory Provide a New Paradigm for Earth Science? Sharper Predictions Using Occam's Digital Razor," *Water Resources Research*, vol. 56, no. 2, p. e2019WR026471, 2020.

[40] M. Amiri *et al.*, "Keras Visualizer," 2023. Software available from https://pypi.org/project/keras-visualizer/.

[41] E. Oostwal, M. Straat, and M. Biehl, "Hidden unit specialization in layered neural networks: ReLU vs. sigmoidal activation," *Physica A: Statistical Mechanics and its Applications*, vol. 564, p. 125517, 2021.

[42] S. R. Dubey, S. K. Singh, and B. B. Chaudhuri, "Activation functions in deep learning: A comprehensive survey and benchmark," *Neurocomputing*, vol. 503, pp. 92–108, 2022.

[43] A. Shrestha and A. Mahmood, "Review of Deep Learning Algorithms and Architectures," *IEEE Access*, vol. 7, pp. 53040–53065, 2019.

[44] F. Chollet *et al.*, "Keras," 2015. Software available from https://keras.io.

[45] M. Abadi, A. Agarwal, P. Barham, E. Brevdo, Z. Chen, C. Citro, G. S. Corrado, A. Davis, J. Dean, M. Devin, S. Ghemawat, I. Goodfellow, A. Harp, G. Irving, M. Isard, Y. Jia, R. Jozefowicz, L. Kaiser, M. Kudlur, J. Levenberg, D. Mané, R. Monga, S. Moore, D. Murray, C. Olah, M. Schuster, J. Shlens, B. Steiner, I. Sutskever, K. Talwar, P. Tucker, V. Vanhoucke, V. Vasudevan, F. Viégas, O. Vinyals, P. Warden, M. Wattenberg, M. Wicke, Y. Yu, and X. Zheng, "TensorFlow: Large-scale machine learning on heterogeneous systems," 2015. Software available from https://tensorflow.org.

[46] R. J. Hyndman and G. Athanasopoulos, *Forecasting: principles and practice*. OTexts, 2018.

[47] C. Voyant, G. Notton, J.-L. Duchaud, L. A. G. Gutiérrez, J. M. Bright, and D. Yang, "Benchmarks for solar radiation time series forecasting," *Renewable Energy*, vol. 191, pp. 747–762, 2022.

[48] N. J. Abram, M. K. Gagan, M. T. McCulloch, J. Chappell, and W. S. Hantoro, "Coral reef death during the 1997 Indian Ocean Dipole linked to Indonesian wildfires," *Science*, vol. 301, no. 5635, pp. 952–955, 2003.

[49] T. R. McClanahan, M. Ateweberhan, C. A. Muhando, J. Maina, and M. S. Mohammed, "Effects of climate and seawater temperature variation on coral bleaching and mortality," *Ecological monographs*, vol. 77, no. 4, pp. 503–525, 2007.

[50] R. Boer and E. Surmaini, "Economic benefits of ENSO information in crop management decisions: case study of rice farming in West Java, Indonesia," *Theoretical and Applied Climatology*, vol. 139, pp. 1435–1446, 2020.

[51] K. A. Hapsari, S. Biagioni, T. C. Jennerjahn, A. Saad, S. Sabiham, M. D. Corre, E. Veldkamp, and H. Behling, "Late Holocene ENSO-related fire impact on vegetation, nutrient status and carbon accumulation of peatlands in Jambi, Sumatra, Indonesia," *Review of Palaeobotany and Palynology*, vol. 293, p. 104482, 2021.

[52] E.-P. Lim and H. H. Hendon, "Causes and predictability of the negative Indian Ocean Dipole and its impact on La Niña during 2016," *Scientific reports*, vol. 7, no. 1, pp. 1–11, 2017.

[53] M. Martono and T. Wardoyo, "Impacts of El Niño 2015 and the Indian Ocean Dipole 2016 on rainfall in the Pameungpeuk and Cilacap regions," in *Forum Geografi*, vol. 31, pp. 184–195, 2017.

[54] B. Lu, H.-L. Ren, A. A. Scaife, J. Wu, N. Dunstone, D. Smith, J. Wan, R. Eade, C. MacLachlan, and M. Gordon, "An extreme negative Indian Ocean Dipole event in 2016: dynamics and predictability," *Climate Dynamics*, vol. 51, pp. 89–100, 2018.

[55] K. H. Brodersen, F. Gallusser, J. Koehler, N. Remy, and S. L. Scott, "Inferring causal impact using Bayesian structural time-series models," *The Annals of Applied Statistics*, pp. 247–274, 2015.

[56] S. H. S. Herho, F. R. Fajary, and D. E. Irawan, "On the Statistical Learning Analysis of Rain Gauge Data over the Natuna Islands," *Indonesian Journal of Statistics and Its Applications*, vol. 6, no. 2, pp. 347–357, 2022.

[57] J. Ma, J. C. P. Cheng, Y. Ding, C. Lin, F. Jiang, M. Wang, and C. Zhai, "Transfer learning for long-interval consecutive missing values imputation without external features in air pollution time series," *Advanced Engineering Informatics*, vol. 44, p. 101092, 2020.

[58] Z. Chen, H. Xu, P. Jiang, S. Yu, G. Lin, I. Bychkov, A. Hmelnov, G. Ruzhnikov, N. Zhu, and Z. Liu, "A transfer Learning-Based LSTM strategy for imputing Large-Scale consecutive missing data and its application in a water quality prediction system," *Journal of Hydrology*, vol. 602, p. 126573, 2021.

[59] K. Ma, D. Feng, K. Lawson, W.-P. Tsai, C. Liang, X. Huang, A. Sharma, and C. Shen, "Transferring hydrologic data across continents–leveraging data-rich regions to improve hydrologic prediction in data-sparse regions," *Water Resources Research*, vol. 57, no. 5, p. e2020WR028600, 2021.

[60] A. Bellagarda, S. Cesari, A. Aliberti, F. Ugliotti, L. Bottaccioli, E. Macii, and E. Patti, "Effectiveness of neural networks and transfer learning for indoor air-temperature forecasting," *Automation in Construction*, vol. 140, p. 104314, 2022.

[61] K. Fang, D. Kifer, K. Lawson, D. Feng, and C. Shen, "The data synergy effects of time-series deep learning models in hydrology," *Water Resources Research*, vol. 58, no. 4, p. e2021WR029583, 2022.